Available online at www.sciencedirect.com
SCIENCE DIRECT®
Biomaterials 27 (2006) 974–985
Biomaterials
www.elsevier.com/locate/biomaterials

3D fiber-deposited scaffolds for tissue engineering: Influence of pores geometry and architecture on dynamic mechanical properties

L. Moroni[a,b,*], J.R. de Wijn[a,b], C.A. van Blitterswijk[a]

[a]*Institute for BioMedical Technology (BMTI), University of Twente, P.O. Box 217, 7500 AE Enschede, The Netherlands*
[b]*IsoTis S.A., P.O. Box 98, 3720 AB Bilthoven, The Netherlands*

Received 14 April 2005; accepted 11 July 2005
Available online 1 August 2005

Abstract

One of the main issues in tissue engineering is the fabrication of scaffolds that closely mimic the biomechanical properties of the tissues to be regenerated. Conventional fabrication techniques are not sufficiently suitable to control scaffold structure to modulate mechanical properties. Within novel scaffold fabrication processes 3D fiber deposition (3DF) showed great potential for tissue engineering applications because of the precision in making reproducible 3D scaffolds, characterized by 100% interconnected pores with different shapes and sizes. Evidently, these features also affect mechanical properties. Therefore, in this study we considered the influence of different structures on dynamic mechanical properties of 3DF scaffolds. Pores were varied in size and shape, by changing fibre diameter, spacing and orientation, and layer thickness. With increasing porosity, dynamic mechanical analysis (DMA) revealed a decrease in elastic properties such as dynamic stiffness and equilibrium modulus, and an increase of the viscous parameters like damping factor and creep unrecovered strain. Furthermore, the Poisson's ratio was measured, and the shear modulus computed from it. Scaffolds showed an adaptable degree of compressibility between sponges and incompressible materials. As comparison, bovine cartilage was tested and its properties fell in the fabricated scaffolds range. This investigation showed that viscoelastic properties of 3DF scaffolds could be modulated to accomplish mechanical requirements for tailored tissue engineered applications.

Keywords: Rapid prototyping; Dynamic mechanical analysis; Scaffolds; Tissue engineering

1. Introduction

Rapid Prototyping techniques have recently attracted more and more interest for applications in tissue engineering as powerful tools to fabricate scaffolds. These scaffolds are built layer by layer, through material deposition on a stage, either in a molten phase (known as fused deposition modeling (FDM)) [1–10] or in droplets together with a binding agent (referred to as 3D Printing) [2–4,11–15]. The 3D outcomes of this process are usually 100% interconnected porous scaffolds per definition, since during fabrication the layers are deposited as interpenetrating networks (material and void, see Fig. 1). Scaffolds have a defined structure and architecture, and can be built with a customized shape by CAD-CAM techniques. This flexibility and versatility in creating scaffolds gives us the opportunity to use rapid prototyping devices to generate improved scaffolds and to study the influence of different structural phenomena on tissue reconstruction. Within this respect, FDM techniques [2,5,10] have been lately used for tissue engineering purposes, offering appealing solutions for scaffold fabrication. Among these devices 3D plotting [16,17] and 3D fiber deposition (3DF) [18] has been recently developed and used for tissue engineering

*Corresponding author. Institute for BioMedical Technology (BMTI), University of Twente, P.O. Box 217, 7500 AE Enschede, The Netherlands. Tel.: +31 302295201; fax: +31 302280255.
E-mail address: l.moroni@tnw.utwente.nl (L. Moroni).

0142-9612/$ - see front matter © 2005 Elsevier Ltd. All rights reserved.
doi:10.1016/j.biomaterials.2005.07.023

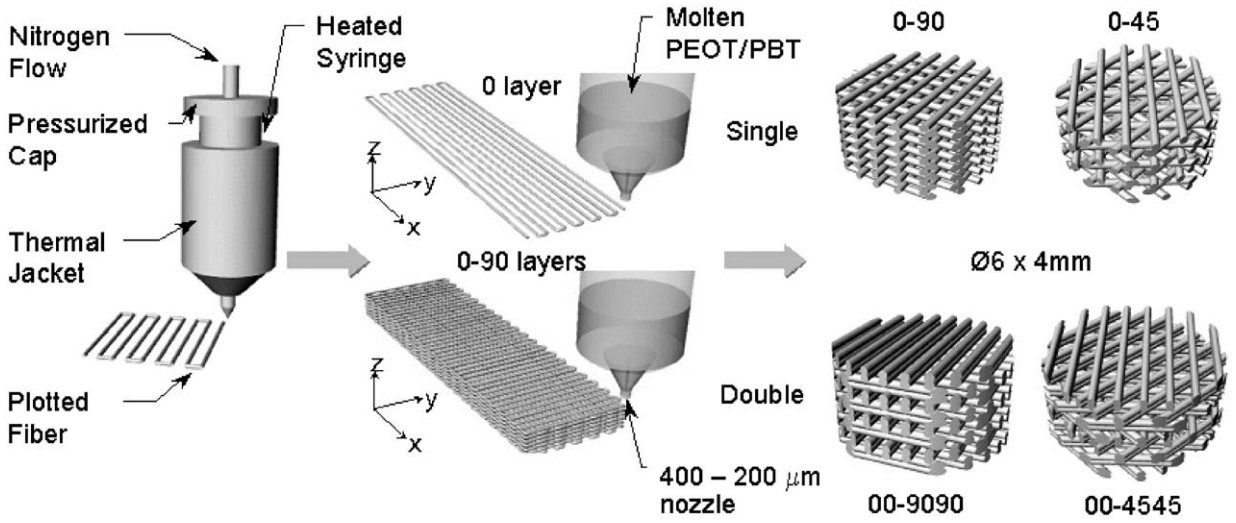

Fig. 1. Draw of a Bioplotter device and 3DF fabrication process. 0–90 and 0–45 scaffolds architectures in single and double layer versions are presented. Modified from Woodfield et al. [18].

purposes, the latter being a system for the extrusion of highly viscous polymers. 3DF is, essentially, a fused deposition technique in which an extrudate of molten polymer is deposited from a XYZ motor drive syringe on a stationary stage by applying pressure.

From a mechanical point of view, one of the main paradigms in tissue engineering and biomechanical science has always been that a scaffold should mimic the biomechanical properties of the organ or tissue to be replaced [14,15,19,20]. Nevertheless, to our knowledge no systematic study has been conducted to assess whether the exact match of mechanical properties is indeed so crucial for optimal tissue regeneration. For instance, since mechanical properties are intimately related to the porosity of porous structures, it might be that a stiffer and less porous scaffold will provide a better integration with the surrounding natural tissue, or—in contrast—that a more flexible and porous one will allow cells to attach and proliferate in a more efficient way. It is here where rapid prototyping offers possibilities to compromise such different requirements into one scaffold, because it adds freedom of varying structural parameters to the non-variable bulk mechanical properties of the material used.

Hence, the aim of this paper was to investigate the dynamic and static mechanical properties of scaffolds with a number of different structural features that can modulate their viscoelastic properties in order to mimic a large collection of natural tissues [21–25]. For this purpose, block-copolymers of polyethyleneoxide-terephtalate (PEOT) and polybutylene-terephtelate (PBT) have been investigated. These polyether-ester multiblock copolymers belong to a class of materials known as thermoplastic elastomers which exhibit good physical properties like elasticity, toughness and strength in combination with easy processability [26]. These properties result mainly from a phase-separated morphology in which soft, hydrophilic PEO segments at environmental temperatures are physically cross-linked by the presence of hard, semi-crystalline PBT segments. In contrast to chemically cross-linked materials, these cross-links are reversible and will be disrupted at temperatures above their glass transition or melting point, vice versa, which gives the material its good processability. This family of copolymers has already been of great interest for tissue engineering and drug delivery applications, because by varying the molecular weight of the starting poly(ethylene glycol) (PEG) segments and the weight ratio of PEOT and PBT blocks it is possible to tailor-make properties, such as wettability [27], swelling [26,28,29], biodegradation rate [29], protein adsorption [30], and mechanical properties [18]. Furthermore, PEOT/PBT block copolymers have shown to be extensively biocompatible both in vitro and in vivo [31–34] and reached clinical applications (PolyActive^{TM}, IsoTis Orthopaedics S.A.) as cement stoppers and bone fillers in orthopedic surgery [35,36]. Being polyether-esters, degradation occurs in aqueous media by hydrolysis and oxidation, the rate of which varying from very low for high PBT contents to medium and high for larger contents of PEOT and longer PEO segments [26,29].

The 3DF scaffolds response was assessed by dynamic mechanical analysis (DMA) since it allows tailoring of test conditions that can more closely simulate the physiological environment of the specific tissue to repair, and it enables scaffolds viscoelastic characterization [37–41]. By varying fiber diameter, fiber spacing and layer thickness in the internal structure of a scaffold, the mechanical properties change. This is due, among other factors, to a correspondent change of the overall porosity of the scaffold. Fiber orientation or deposition angle are also parameters to consider. If the angle step

with which two subsequent layers are deposited or if the number of layers plotted with the same orientation on top of each other is varied, a different mechanical behavior will result at constant porosity. Bovine articular cartilage was tested as a reference to show how a scaffold structure can be tailored to mimic the biomechanical behavior of a specific tissue. Therefore, the combination of 3DF and DMA is shown in this study to be a powerful tool to achieve optimized scaffolds for tissue engineering applications.

2. Materials and methods

2.1. Scaffold fabrication

PEOT/PBT block copolymers were obtained from IsoTis S.A. (Bilthoven, The Netherlands). Their chemical composition is represented by the notation aPEOTbPBTc, where a is the molecular weight of the starting PEG segments used in the polymerization process, while b and c refer to the weight ratio between PEOT and PBT blocks, respectively. For this study, 300PEOT55PBT45 co-polymer was used.

3D scaffolds were fabricated with a Bioplotter device (Envisiontec GmbH, Germany), essentially an XYZ plotter construction as previously described by Landers et al. [17]. A few modifications enabled the extrusion of highly viscous 300PEOT55PBT45 melts, as shown in Fig. 1. Briefly, the polymer was placed in a stainless steel syringe and heated at $T = 190\,^{\circ}\mathrm{C}$ through a heated cartridge unit, mounted on the "X"-mobile arm of the apparatus. When the polymer reached a molten phase, a nitrogen pressure of 5 bar was applied to the syringe through a pressurized cap. Rectangular block models were loaded on the Bioplotter CAD/CAM software and plotted layer by layer, through the extrusion of the polymer on a stage as a fiber. The scaffold was then characterized by varying the fiber diameter ($d1$) (through the nozzle diameter or the deposition speed), the spacing between fibers in the same layer ($d2$), the layer thickness ($d3$) and the configuration of the deposited fibers within the whole architecture, which are all parameters set on the CAD/CAM software controlling the Bioplotter. The nozzles used to extrude polymer fibers were stainless steel Luer Lock hypodermic needles with internal diameter (ID) of 400 and 200 μm, shortened to a length of approximately 16.2 mm. The corresponding plotted fibers had a diameter $d1$ of 260 and 170 μm, respectively. The fiber spacing $d2$ was set to 600, 800 and 1000 μm, and the layer thickness $d3$ was originally set to 150, 250 and 350 μm. Since the adhesion of fibers between two subsequent layers was compromised for a layer thickness larger than 60% of the fiber diameter value, $d3 = 275\,\mu\mathrm{m}$ was chosen as the largest value for $d1 = 170\,\mu\mathrm{m}$ set of scaffolds. The architecture was changed by plotting fibers with 45° and 90° angle steps between two successive layers (called 0–45 and 0–90 configurations, respectively) and by modifying the fiber orientation after one or two printed layers (referred to as single and double layers configurations, respectively). The deposition speed was varied between 100 and 300 mm/min in order to assess its influence on fiber diameter and overall porosity of the scaffolds.

For comparison with more conventional techniques, scaffolds were also made by salt leaching, whereby a mixture of polymer powder and salt particles was compression molded into blocks and the salt removed by leaching in water. The average pore size of these scaffolds was 182 μm, with a maximum pore size of 600 μm and an overall porosity of 75% [42–43].

2.2. Scaffold characterization

Cylindrical plugs of 6 mm in diameter by 4 mm in height were cored out in the "Z-direction" from the rectangular 3D plotted blocks, and taken as samples for the mechanical analysis. Scaffolds geometry and architecture were characterized by scanning electron microscopy (SEM) analysis with a Philips XL 30 ESEM-FEG. Samples were gold sputtered (Cressington) before SEM analysis. The porosity of 3D plotted scaffolds was calculated following the theoretical approach by Landers et al. [17]:

$$P = 1 - \frac{V_{\mathrm{scaffold}}}{V_{\mathrm{cube}}} = 1 - \frac{\pi}{4}\frac{d_1^2}{d_2 d_3}, \tag{1}$$

where P is the scaffold porosity, $d1$ the fiber diameter, $d2$ the fiber spacing and $d3$ the layer thickness, within each different structure (see also Tables 1 and 2).

Porosity was also experimentally measured—e.g. in case of the salt-leached scaffolds—by analyzing the mass and the volume of each scaffold, as

$$P = 1 - \frac{M}{V}\frac{1}{\rho}, \tag{2}$$

where M and V are the measured mass and volume of the scaffolds, while ρ is the specific density of 300PEOT55PBT45 ($1.2\,\mathrm{g/cm^3}$). Since, there was only a small difference ($<1\%$) between theoretical and experimental porosities (data not shown), we decided to refer to the theoretical one, as more conformal to the fabrication parameters of the Bioplotter.

2.3. Bovine articular cartilage harvest

Bovine articular cartilage plugs of the same dimension as the 3D scaffolds specimens were punched out from the knee of a 6-month old calf. The obtained samples were perpendicularly sectioned. Once the knee was opened, cartilage plateaus were kept hydrated with phosphate-buffered saline (PBS) (Gibco-BRL), while the cylindrical plugs were punched out from the femoral condyle with a coring drill. The samples were then stored in PBS and mechanically tested during the same day.

2.4. Dynamic mechanical analysis

A DMA instrument (Perkin Elmer 7e) was used to evaluate the viscoelastic properties of the 3D scaffolds and of the bovine articular cartilage cylindrical plugs. For each structural and architectural configuration three samples were tested in all the experiments performed. In the case of bovine articular cartilage, six plugs were tested to level out the differences between the different regions of the femoral plateau, where the samples were taken. Cylindrical fixtures

Table 1
Elastic properties of few different 3DF PEOT/PBT scaffolds with a 00-9090 architecture and bovine articular cartilage, tested with DMA

Porosity (%)	Scaffold structure (μm)	E' (MPa)—Dry	E'' (MPa) – PBS	E' (MPa)—PVP	Ha (MPa)—Dry	Ha (MPa) – PBS	Ha (MPa)—PVP
28.9	$d_1 = 260$, $d_2 = 800$, $d_3 = 150$, $V = 100$	13.7±2.63	—	—	8±1.47	—	—
41	$d_1 = 260$, $d_2 = 600$, $d_3 = 150$	8.66±0.81	8.74±2.44	9.7±0.5	6.88±0.81	4.88±0.23	6.33±1.47
55.8	$d_1 = 260$, $d_2 = 300$, $d_3 = 150$	6.63±0.83	7.1±0.66	5.28±1.35	4.73±0.88	2.35±0.12	3.27±1.2
64.2	$d_1 = 260$, $d_2 = 1000$, $d_3 = 150$	2.6±0.23	2.75±2.68	2.6±0.02	0.66±0.25	2±0.12	1.59±0.02
78.7	$d_1 = 260$, $d_2 = 1000$, $d_3 = 250$	0.815±0.11	1.21±1.08	1.01±0.99	0.24±0.11	0.43±0.08	0.58±0.3
85.4	$d_1 = 170$, $d_2 = 600$, $d_3 = 275$	0.589±0.11			0.04±0.005		
91.2	$d_1 = 170$, $d_2 = 1000$, $d_3 = 275$	0.262±0.09			0.13±0.01		
Bovine cartilage (65–80)	—	—	9.3±0.9	9.64±1.81	—	0.49±0.05	0.64±0.16

Table 2
Plastic properties of few different 3DF PEOT/PBT scaffolds with a 00-9090 architecture and bovine articular cartilage, tested with DMA

Porosity (%)	Scaffold structure (μm)	Tan δ—dry	Tan δ—PBS	Tan δ—PVP	ε (%)—dry	ε (%)—PBS	ε (%)—PVP
28.9	$d_1 = 260$, $d_2 = 800$, $d_3 = 150$, $V = 100$		—	—	0.36±0.13	—	—
41	$d_1 = 260$, $d_2 = 600$, $d_3 = 150$	0.075±0.011	0.065±0.004	0.064±0.002	0.55±0.001	0.72±0.27	0.71±0.28
55.8	$d_1 = 260$, $d_2 = 800$, $d_3 = 150$	0.077±0.002	0.084±0.005	0.067±0.0007	0.91±0.07	1.12±0.62	0.7±0.43
64.2	$d_1 = 260$, $d_2 = 1000$, $d_3 = 150$	0.107±0.011	0.111±0.05	0.091±0.01	2.37±0.93	1.49±0.27	1.7±0.1
78.7	$d_1 = 260$, $d_2 = 1000$, $d_3 = 250$	0.182±0.009	0.155±0.05	0.121±0.019	14.56±1.07	7.59±1.26	17.38±0.59
85.4	$d_1 = 170$, $d_2 = 600$, $d_3 = 275$	0.18±0.003	—	—	49.67±15.9	—	—
91.2	$d_1 = 170$, $d_2 = 1000$, $d_3 = 275$	0.189±0.014	—	—	44.72±8.44	—	—
Bovine cartilage (65–80)	—	—	0.164±0.005	0.175±0.03	—	27.16±12.05	46.91±9.86

were chosen to test the specimens along their compression axis, in the "*Z*-direction".

Dynamic stress and creep recovery tests were performed on scaffolds for mechanical characterization. In the dynamic stress test, scaffolds were loaded with a dynamic force varying from 3.5 to 4.5 N, which is well in the middle of the linear part of the static stress–strain curve. A ramp of 50 mN/min at a constant frequency of 1 Hz was used, as depicted in Fig. 2. Dynamic stiffness, or storage modulus, and damping factor, or tan δ, were calculated.

In the creep recovery test, samples were pre-loaded with a recovery force of 100 mN for 2 min. Then, a force of 3.5 N was applied instantaneously and kept for 3 min, after which the loading condition was returned to the recovery value. This set up was cycled for three times to ensure that no significant difference was experienced after each loading cycle, in terms of equilibrium modulus and unrecovered creep strain. The same experiment was repeated with a loading force of 4.5 N to assess creep and recovery properties of the fabricated scaffolds in the minimum and maximum force range applied in the dynamic stress analysis.

For a frequency scan test, a force of 100 mN was applied and kept constant, while a variable load of 80 mN was superimposed with a frequency sweep from 0.1 to 15 Hz. The elastic modulus and dynamic viscosity were measured and related to the viscoelastic behavior of the scaffolds as the frequency increases.

To consider the influence of an aqueous environment and possible perfusion effects, the tests were done in three different environmental conditions: in a nitrogen atmosphere, in PBS and in a synovium-like fluid. This last wet setting consisted of a 3% (w/v) solution of polyvinilpyrrolidone (PVP) in de-ionized water. The dynamic viscosity of the solution was measured with Brookfield viscosimeter and determined as 0.01 Pa s, which is in the range of natural synovium fluid [44]. Bovine articular cartilage was tested only in wet milieus. Scaffolds were soaked both in PBS and in PVP-solution over night, before loading. The temperature was set to 37 °C for all the experiments.

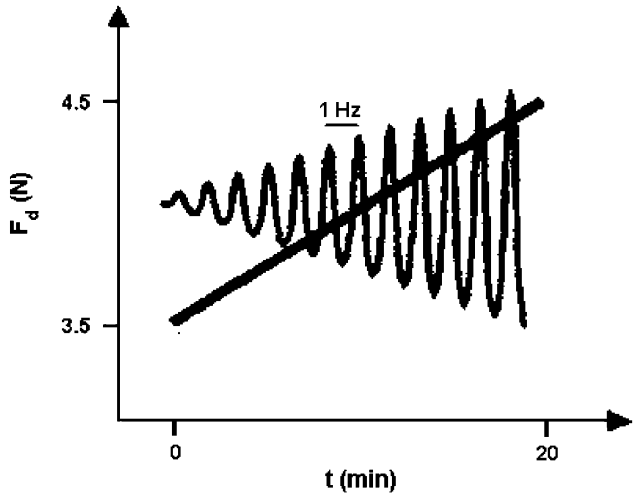

Fig. 2. Schematic diagram of the dynamic force applied on 3D scaffolds during viscoelastic assessment.

2.5. Poisson's ratio optical measurement

Poisson's ratios of scaffolds, bulk polymer and bovine articular cartilage were measured through an optical technique as described by Jurvelin et al. [45]. Briefly, samples were placed between non-rotating tips of a micrometer under a stereomicroscope. Original height and diameter were measured. Then, a compressive strain of 10% was applied to the specimens through the micrometer and the final height and diameter were determined, after leaving the samples equilibrating for 1 h. Dimensional measurements were performed through imaging analysis (Scion Image, Scion Corporation) of micrographs acquired with a video camera (Sony progressive 3CCD) and a frame grabber (PCImage SRGB, Matrix Vision) connected to the stereomicroscope. Poisson's ratios were then computed as:

$$v = -\frac{\Delta D/D}{\Delta L/L}, \tag{3}$$

where v is the Poisson's ratio, D and L are the samples original diameter and height, respectively, while ΔD and ΔL the variation of diameter and length between the unstrained and the strained configurations.

From the measured experimental values of dynamical stiffness and Poisson's ratio, scaffolds shear modulus was indirectly calculated through the formula:

$$G = \frac{E}{2(1-v)}, \tag{4}$$

where G is the scaffold shear modulus and E the dynamic stiffness.

3. Results

3.1. Scaffolds characterization

300PEOT55PBT45 3D scaffolds with different pore architecture and geometry were fabricated. Pore architecture was dependent on fiber orientation and deposition (Fig. 3). A fiber deposition angle of 90° created quadrangular pores (Fig. 3a–c), while a 45° angle step generated polygonal pores (Fig. 3d–f). Furthermore, the deposition of two successive layers with the same fiber orientation resulted in doubling the pore height (Fig. 3c and f). The pore geometry was defined by fiber diameter and spacing ($d1$ and $d2$), and layer thickness ($d3$) (Fig. 3c). A decrease of the fiber diameter from 260 to 170 μm and a decrease of the layer thickness from 350 to 150 μm corresponded to a decrease of the pore height. Analogously, a decrease of the fiber spacing from 1000 to 600 μm lead to a decrease of the pore width. The pore height was mainly defined by the layer thickness, while the pore width was defined by the difference between fiber spacing and fiber diameter. The effect of deposition speed (V) on fiber diameter and ultimately on scaffold

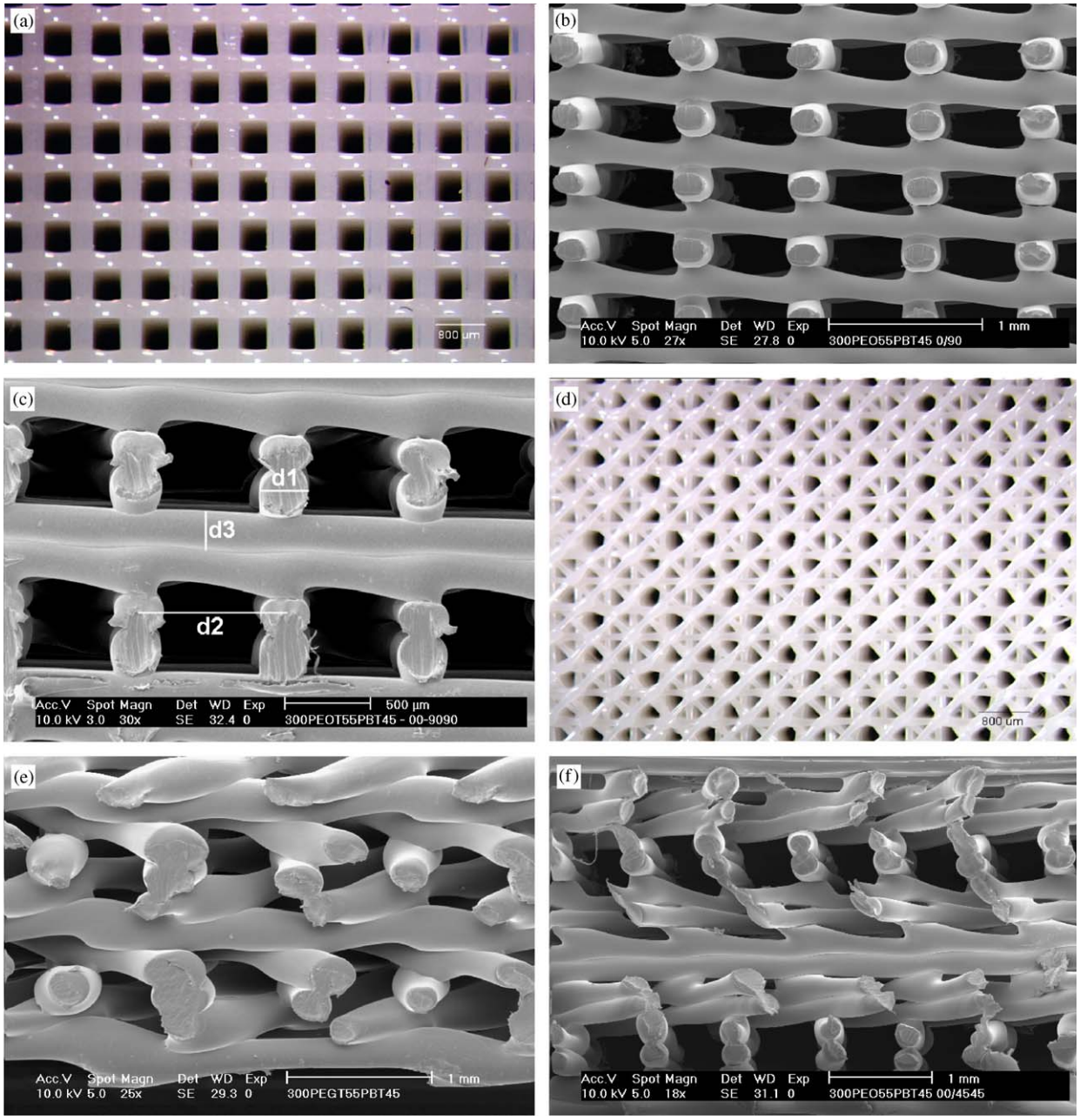

Fig. 3. Optical microscopy pictures of scaffolds surface and SEM micrographs of cross sections. (d–f) 0–45 and (a–c) 0–90 architecture configurations in (b, e) single and (c, f) double layer versions. (c) represents graphically the fiber diameter and spacing ($d1$ and $d2$) and the layer thickness $d3$ of a 3DF scaffold

porosity is depicted in Fig. 4. A decrease of V from 300 to 100 mm/min resulted in an increase of the fiber diameter from $268 \pm 32\,\mu m$ to $432 \pm 40\,\mu m$, which corresponded to a decrease of the scaffold's porosity from $75\% \pm 6\%$ to $29\% \pm 13\%$. The variation of all the parameters above introduced, one by one, allowed to create a set of scaffolds within a porosity range from 29% up to 91%.

SEM analysis revealed a significant consistency between the theoretical and real values of fiber diameter, fiber spacing, and layer thickness for all the scaffolds processed. The fiber diameter ($d1$) was $268 \pm 32\,\mu m$ when the larger Bioplotter tip (ID = 400 µm) was used and $170 \pm 15\,\mu m$ when the smaller one was used (ID = 200 µm). The fiber spacing ($d2$) was 605 ± 12, 807 ± 28, and $1001 \pm 0.00\,\mu m$. The layer thickness ($d3$) was 148 ± 10, 257 ± 11, and $344 \pm 11\,\mu m$. All the scaffolds produced had 100% pore interconnectivity and no layer delamination phenomenon occurred in the porosity range analyzed.

3.2. Dynamic mechanical properties

3D plotted scaffolds were tested to characterize their viscoelastic behavior. Tables 1 and 2 summarize the obtained data from DMA on some of the deposited scaffolds with different porosity, and on articular bovine cartilage. With increasing porosity and/or by changing the scaffold architecture, the dynamic stiffness increased from a minimum value of 0.186 ± 0.005 MPa to a maximum of 13.7 ± 2.63 MPa (Table 1, columns 3–5), while the equilibrium modulus varied from 0.04 ± 0.005 to 8 ± 0.81 MPa (Table 1, columns 6–8). Analogously, the damping factor decreased from 0.202 ± 0.015 to 0.075 ± 0.012 (Table 2, columns 3–5), while the creep uncovered strain changed from $49.67 \pm 15.9\%$ to $0.36 \pm 0.13\%$ in the same porosity series (Table 2, columns 6–8). Dynamic stiffness and equilibrium modulus of bovine articular cartilage were higher under synovium-like fluid conditions and measured as 9.64 ± 1.81 and 0.64 ± 0.16 MPa, respectively. Damping factor and creep unrecovered strain were $0.175 \pm 0.03\%$ and $46.91 \pm 9.86\%$. DMA showed an increase in dynamic stiffness and equilibrium modulus with decreasing fiber spacing and layer thickness (Figs. 5a and b). Inversely, the damping factor and the uncovered creep strain decreased, which resulted in a less plastic behavior of the scaffolds (Figs. 5c and d). The influence of the architecture on the mechanical properties of the scaffolds was also studied (Fig. 6). By varying the layer configuration from single to double layer printed versions and from 0–90 to 0–45 fiber orientation, the dynamic stiffness and the equilibrium modulus decreased (Figs. 6a and b), while the damping factor and the unrecovered creep strain increased (Figs. 6c and d),

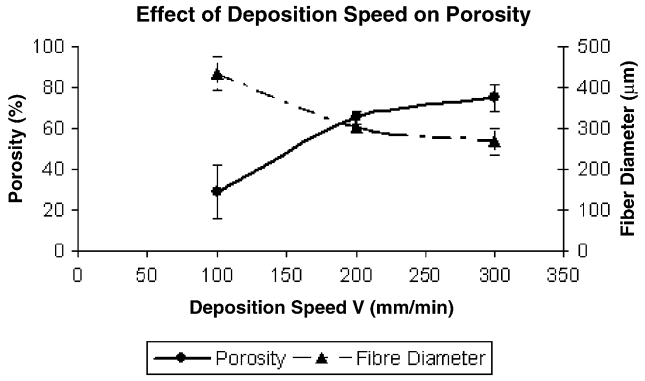

Fig. 4. Effect of deposition speed on scaffolds porosity and fiber diameter in a 00–9090 layer configuration with an ID = 400 μm nozzle.

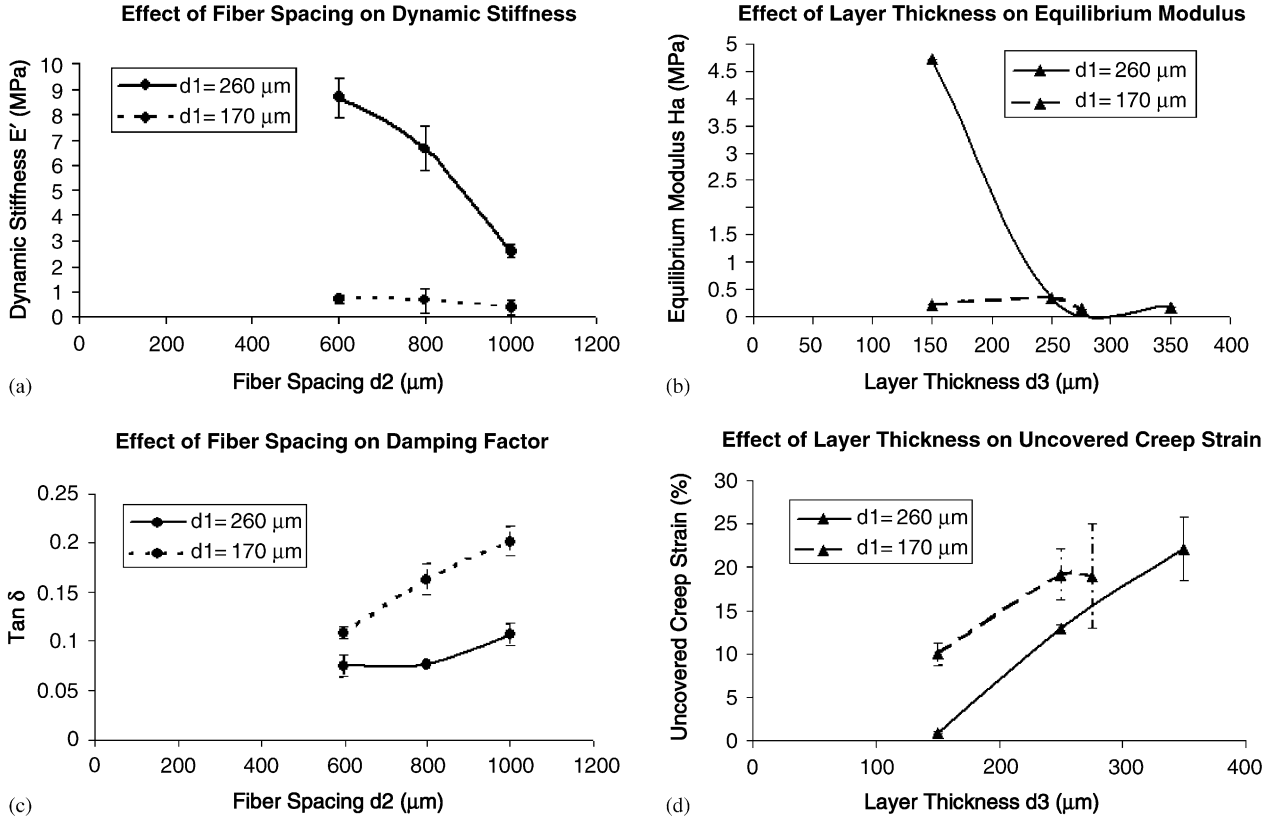

Fig. 5. Effect of (a, c) fibre spacing and (b, d) layer thickness on, respectively, elastic and plastic behavior of 300PEGT55PBT45 3D scaffolds. Analogous trend were found concerning the influence of layer thickness and fibre spacing on the elastic and plastic behavior, respectively. 00–9090 scaffold configuration was fixed.

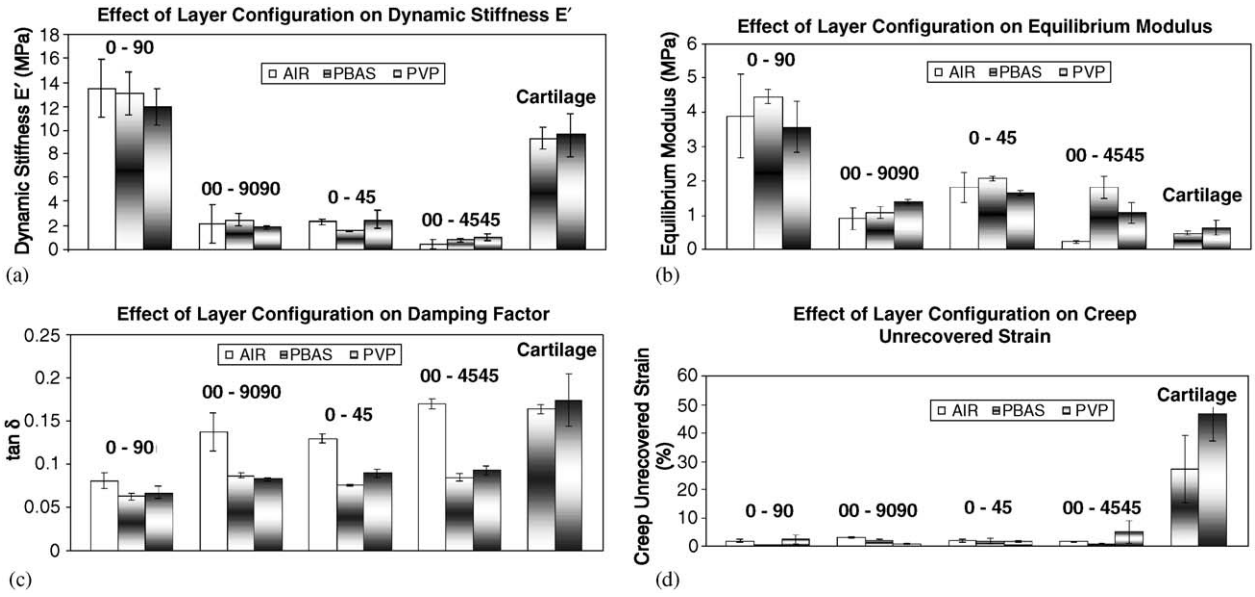

Fig. 6. Effect of scaffold architecture at a constant porosity $P = 75\%$ on (a, b) elastic and (c, d) plastic behavior of 3DF scaffolds in different media. Bovine articular cartilage was also tested with the same loading protocol as a reference.

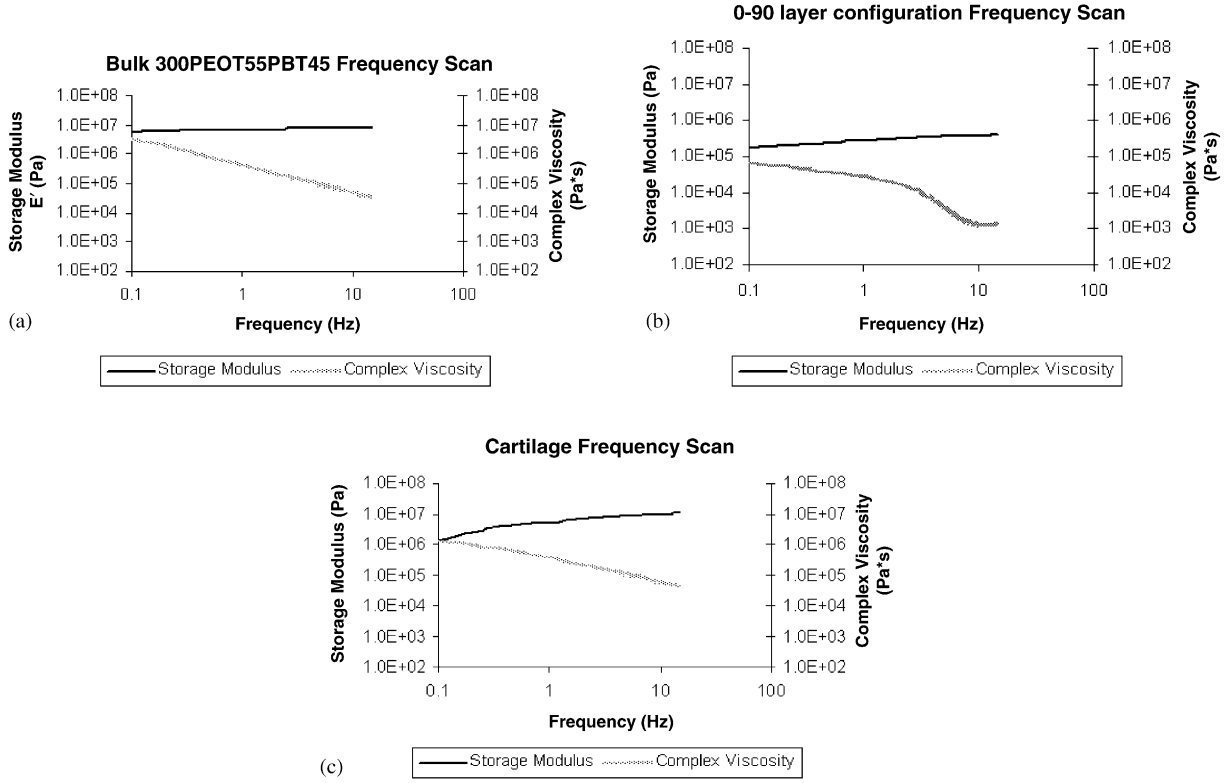

Fig. 7. Frequency scan diagram for 300PEGT55PBT45 bulk and 0–90 scaffolds, and bovine articular cartilage. An increase of applied load frequency generates a decrease of dynamic viscosity and an increase of dynamical stiffness, which is characteristic of viscoelastic materials. Similar behavior was shown for all the other scaffold architectures.

although the porosity remained constant to 75%. These results were then used to make a comparison with the mechanical data on bovine articular cartilage. A frequency scan of bovine articular cartilage, solid material and 3DF scaffolds has also been performed and depicted in Fig. 7. This test further assessed the modulation of viscoelastic properties of 300PEOT55PBT45 along a frequency span typical of

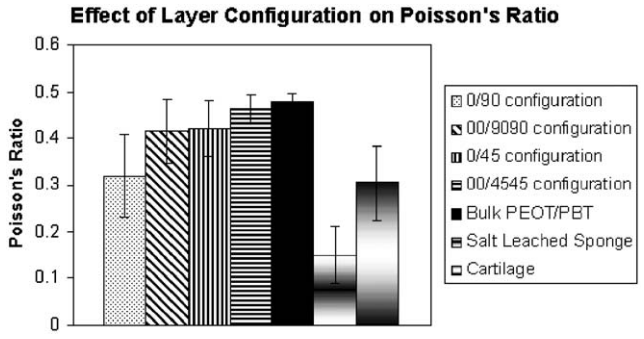

Fig. 8. Influence of scaffold architecture on Poisson's ratio optical measurement. Bulk and salt-leached PEOT/PBT scaffold, and bovine articular cartilage were also tested as references to show architectural compressibility modulation.

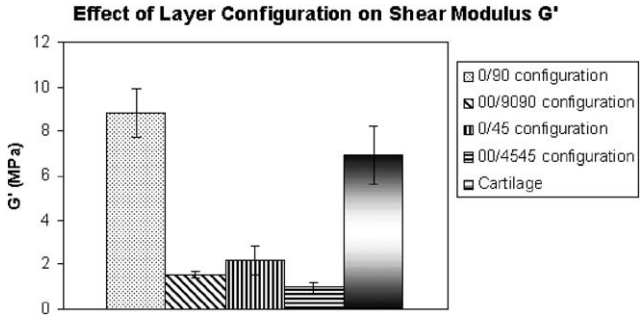

Fig. 9. Effect of scaffold architecture on shear modulus, indirectly calculated from Poisson's ratio and dynamic stiffness measurements.

physiological conditions [21], since bovine articular cartilage values were found in between solid material and 3DF scaffolds.

Results from the optical measurement of Poisson's ratio of scaffolds with different architectures are shown in Fig. 8. A modulation from 0.117 ± 0.06 to 0.478 ± 0.015 by varying the scaffolds architecture or by increasing their porosity was measured. Correspondently, the shear modulus G' increased from 0.96 ± 0.26 to 8.81 ± 1.1 MPa (Fig. 9). Poisson's ratio of cartilage was 0.305 ± 0.08 (Fig. 8), and the shear modulus was 6.93 ± 1.3 MPa (Fig. 9). All the viscoelastic parameters were measured along the main compression axis of the structures, in the "Z-direction". Therefore, from the mechanical characterization performed we cannot infer any information in the other directions, since both the fabricated scaffolds and natural cartilage are anisotropic structures.

4. Discussion

In this study, the modulation of the viscoelastic properties of 3D fiber deposited PEOT/PBT scaffolds has been investigated. Bovine articular cartilage was also studied as a reference to show how 3DF scaffolds can mimic a natural tissue. Firstly, SEM analysis revealed a very good consistency between the machine settings and the actual parameters. Variations of fiber diameter, fiber spacing and layer thickness were due to a decrease of polymer melt viscosity over time as a result of thermal degradation. This implied a faster polymer flow out of the tip during printing, and consequently a slight increase of fiber diameter at a specific deposition speed. Nevertheless, scaffolds presented 100% interconnected pores and were reproducible with the same characteristics each time they were processed.

3DF constructs were mechanically characterized through DMA for different geometrical and architectural configurations. From a mechanical point of view, these scaffolds were treated and analyzed following a solid-state mechanics approach. However, it has to be noted that the macroporous structure plays a determinant role on the properties of the whole scaffold. It is, indeed, the organization and the volume of macropores that drives the modulation of mechanical properties from the bulk material. Dynamic stress and creep recovery tests determined the constructs' dynamic (dynamic stiffness and damping factor) and quasi-static (equilibrium modulus and creep unrecovered strain) behavior, respectively. Dynamic stiffness and equilibrium modulus increased with decreasing fiber spacing and layer thickness. Inversely, the damping factor and the creep unrecovered strain decreased, illustrating a less plastic behavior of the scaffolds (see Fig. 5). The observed trends are directly related to the scaffold porosity. In fact, a decrease of fiber diameter, fiber spacing or layer thickness results in an increase of deposited polymer and a consequent decrease of pore volume within the same scaffold volume. A similar trend was also obtained by decreasing the fiber deposition speed. In this case, a decrease in the deposition speed resulted in a larger polymer flow per traveled distance, which implied a larger fiber diameter and lead to a decrease of porosity. As shown in Tables 1 and 2, a slight increase in dynamic stiffness and equilibrium modulus, and a consequent small decrease in the viscous factors was generally experienced from dry to wet conditions. Such an environment, as in a physiological setting, introduces a second phase during dynamical load. The final measurement is then the sum of the response of the material itself and that of a fluid phase being transported in and out of the solid phase through the pores. The result is an increase of the apparent stiffness at higher fluid phase viscosities. In the case of the viscous factors such a biphasic liquid–solid system implied a decrease of damping and unrecovered creep strain, because part of the lost energy during load is dissipated by the liquid component. This viscoelastic behavior is also encountered in many natural tissues and is strictly connected to the macro porous structure of the

constructs. In fact, a larger pore volume leads to an increase of the mechanical response of the fluid component, since more liquid will be pumped through the pores of the scaffold.

The modulation of PEOT/PBT 3DF scaffolds viscoelastic properties was also found for different pore architecture, while the porosity was kept constant. Interestingly, a change in the scaffold from single to double layer configuration and from 0–90 to 0–45 fiber deposition resulted in a more flexible and plastic construct, while the porosity was constant (see Fig. 6). In the first case, we could infer that an increase in the pore size along the compression axis led to a mechanically weaker structure. In the second case the local increase of contact points between fibers implied a larger contact area and, thus, a decrease of the local stress experienced by the structure. This was reflected in lower values of storage and equilibrium modulus. Again, a decrease in dynamic stiffness was accompanied by an increase of the damping factor, which implied a more plastic behavior of the scaffolds. However, while the equilibrium modulus varied in a similar way as the dynamic stiffness, the creep-unrecovered strain did not significantly change with the architecture and was considerably low for the fixed porosity analyzed.

A further assessment of the mechanical modulation of PEOT/PBT scaffolds was given by the frequency scan test (Fig. 7). In this case, the higher the frequency with which the force was dynamically applied, the higher was the storage modulus (dynamic stiffness), but the lower the dynamic viscosity. A comparison between frequency scans of bulk polymer, scaffolds, and bovine articular cartilage reveals an enhanced viscoelastic behavior for the 3D structure as compared to the bulk one, the plastic nature of bovine articular cartilage being even more pronounced than the copolymer.

Concerning the compressibility of the scaffold, the Poisson's ratio has been measured for solid material, salt-leached and 3DF copolymer scaffolds. Poisson's ratios generally vary between 0 and 0.5. In this range, the lower its value, the more compressible is a material. A comparison of the measured ratios between the fabricated scaffolds revealed a compressibility that is controlled by their architecture and structure. In particular, a tendency to higher values of Poisson's ratio for double layer and 0–45 configurations of the scaffolds could be detected with respect of single layer and 0–90 versions. Therefore, doubling the printed layers with the same angle orientation or decreasing the angle orientation step to 45° resulted in less compressible scaffolds at constant porosity (see Fig. 8).

Similar implications as for dynamic stiffness and equilibrium modulus can be found for the shear modulus. Doubling the printed layers with the same angle orientation or changing the layer orientation angle step from 90° to 45°, led to less stiff scaffolds (Fig. 9). An increase in pore dimension along the compression axis implied a more flexible structure in that direction and apparently also in the perpendicular plane, where the shear stress is experienced. A larger contact area between the fibers, as previously described, characterizes the 0–45 scaffold configuration. Apparently, this affects the local stress field so that a lower shear modulus is found.

A first comparison between the mechanical parameters measured for 3D scaffolds and bovine cartilage revealed that a 0–90 layer configuration of the deposited fibers was most effective in mimicking the biomechanical behavior of the natural tissue with this specific copolymer. It is certainly true that in this scenario the great freedom that 3D fiber deposition offers as a fabrication device, allows one to customize and render scaffolds for a wide variety of tissue engineering applications. It was the aim of this investigation to show how a number of mechanical parameters of 3D scaffolds can be controlled, simply by varying their structure and architecture. Evidently, the bulk properties of the material used plays a major role on the overall behavior of 3D porous scaffolds. In this respect, the PEOT/PBT copolymers give the possibility to look at the effect of bulk properties on 3D porous constructs by changing the copolymer composition. Therefore, our following studies will be directed to superimpose bulk polymer properties of other PEOT/PBT copolymers on the current structural findings.

5. Conclusions

This study shows how viscoelastic properties of 3D fiber deposited PEOT/PBT blocks copolymer scaffolds could be modulated to accomplish mechanical requirements for tailored tissue engineered applications. The modulation was not only dependent on porosity, but also on fiber deposition and orientation. The scaffold architecture is relevant from a biological point of view, since pores size and shape influence cells attachment and in growth. The 3DF-Bioplotter device is able to fabricate structures with high reproducibility and flexibility, and it offers a wide variety of solutions in terms of different architectural and geometrical configurations. DMA enables tailoring 3D fiber deposition fabrication parameters in order to optimize scaffolds architecture and structure.

Acknowledgements

Discussion on 3D fiber deposition with T.B.F. Woodfield was really appreciated. We are also grateful to P. Kaim for measuring the dynamic viscosity of the

synovium-like fluid. F. Peters was very helpful in setting the DMA equipment.

References

[1] Cooke MN, Fisher JP, Dean D, Rimnac C, Mikos AG. Use of stereolithography to manufacture critical-sized 3D biodegradable scaffolds for bone ingrowth. J Biomed Mater Res Part B: Appl Biomater 2002;64B:65–9.
[2] Hutmacher DW. Scaffold design and fabrication technologies for engineering tissues—state of the art and future perspectives. J Biomater Sci Polymer Edn 2002;12(1):107–24.
[3] Hutmacher DW. Scaffolds in tissue engineering bone and cartilage. Biomaterials 2000;21:2529–43.
[4] Sachlos E, Czernuszka JT. Making tissue engineering scaffolds work. Review on the application of solid freeform fabrication technology to the production of tissue engineering scaffolds. Eur Cells Mater 2003;5:29–40.
[5] Hutmacher DW, Schantz T, Zein I, Ng KW, Teoh SH, Tan KC. Mechanical properties and cell cultural response of polycaprolactone scaffolds designed and fabricated via fused deposition modelling. J Biomed Mater Res 2001;55:203–16.
[6] Vozzi G, Flaim C, Ahluwalia A, Bhatia S. Fabrication of PLGA scaffolds using soft lithography and microsyringe deposition. Biomaterials 2003;24:2533–40.
[7] Vozzi G, Previti A, De Rossi D, Ahluwalia A. Microsyringe-based deposition of two-dimensional and three-dimensional polymer scaffolds with a well-defined geometry for application to tissue engineering. Tissue Eng 2002;8(6):1089–98.
[8] Woodfield TBF, Bezemer JM, Pieper JS, van Blitterswijk CA, Riesle J. Scaffolds for tissue engineering of cartilage. Crit Rev Eukar Gene Expression 2002;12(3):209–36.
[9] Yang S, Leong KF, Du Z, Chua CK. The design of scaffolds for use in tissue engineering. Part II. Rapid prototyping techniques. Tissue Eng 2002;8(1):1–11.
[10] Zein I, Hutmacher DW, Tan KC, Teoh SH. Fused deposition modelling of novel scaffold architectures for tissue engineering applications. Biomaterials 2002;l23:1169–85.
[11] Sachs E, Brancazio D, Bredt JF, Tuerck H, Lee Sang-J-On J, Curodeau A, Khanuja S, Cima M, Fan A, Michaels SP, Lauder A. Three-dimensional printing techniques. International Patent WO 9325336, 1993.
[12] Giordano RA, Wu BM, Borland SW, Cima LG, Sachs EM, Cima MJ. Mechanical properties of dense polylactic acid structures fabricated by three dimensional printing. J Biomater Sci Polymer Edn 1996;8(1):63–75.
[13] Kim SS, Utsunomiya H, Koski JA, Wu BM, Cima MJ, Sohn J, Mukai K, Griffith LG, Vacanti JP. Survival and function of hepatocytes on a novel three-dimensional synthetic biodegradable polymer scaffold with intrinsic network of channels. Ann Surg 1998;228(1):8–13.
[14] Sherwood JK, Riley SL, Palazzolo R, Brown SC, Monkhouse DC, Griffith LG, Landeen LK, Ratcliffe A. A three-dimensional osteochondral composite scaffold for articular cartilage repair. Biomaterials 2002;23:4739–51.
[15] Taboas JM, Maddox RD, Krebsbach PH, Hollister SJ. Indirect solid free form fabrication of local and global porous, biomimetic and composite 3D polymer-ceramic scaffolds. Biomaterials 2003;24:181–94.
[16] Landers R, Hübner U, Schmelzeisen R, Müllhaupt R. Rapid prototyping of scaffolds derived from thermoreversible hydrogels and tailored for application in tissue engineering. Biomaterials 2002;23:4437–47.
[17] Landers R, Pfister A, Hübner U, John H, Schmelzeisen R, Müllhaupt R. Fabrication of soft tissue engineering scaffolds by means of rapid prototyping techniques. J Mater Sci 2002; 37:3107–16.
[18] Woodfield TBF, Malda J, de Wijn J, Péters F, Riesle J, van Blitterswijk CA. Design of porous scaffolds for cartilage tissue engineering using a three-dimensional fibre-deposition technique. Biomaterials 2004;25:4149–61.
[19] Hollister SJ, Maddox RD, Taboas JM. Optimal design and fabrication of scaffolds to mimic tissue properties and satisfy biological constraints. Biomaterials 2002;23:4095–103.
[20] Lin ASP, Barrows TH, Cartmell SH, Guldberg RE. Microarchitectural and mechanical characterization of oriented porous polymer scaffolds. Biomaterials 2003;24:481–9.
[21] van Mow C, Ratcliffe A, Poole AR. Cartilage and diarthrodial joints as paradigms for hierarchical materials and structures. Biomaterials 1992;13(2).
[22] Laasanen MS, Töyräs J, Korhonen RK, Rieppo J, Saarakkala S, Nieminen MT, Hirvonen J, Jurvelin JS. Biomechanical properties of knee articular cartilage. Biorheology 2003;40:133–40.
[23] Doerhing TC, Carew EO, Vesely I. The effect o strain rate on the viscoelastic response of aortic valve tissue: a direct-fit approach. Ann Biomed Eng 2004;32(2):223–32.
[24] Elhadj S, Chan R, Forsten-Williams K. Implementation of an optical method for the real-time determination of uniaxial strain and vessel mechanics. IEEE Trans Biomed Eng 2004; 51(3):536–8.
[25] Yeni YN, Christopherson GT, Turner AS, Les CM, Fyhrie DP. Apparent viscoelastic anisotropy as measured from nondestructive oscillatory tests can reflect the presence of a flaw in cortical bone. J Biomed Mater Res 2004;69A(1):124–30.
[26] Bezemer JM, Grijpma DW, Dijkstra PJ, van Blitterswijk CA, Feijen J. A controlled release system for proteins based on poly(ether ester) block-copolymers: polymer network characterization. J Control Release 1999;62(3):393–405.
[27] Olde Riekerink M, Claase M, Engbers G, Grijpma D, Feijen J. Gas Plasma etching of PEO/PBT segmented block copolymer films. J Biomed Mater Res 2003;65A(4):417–28.
[28] van Dijkhuizen-Radersma R, Peters FL, Stienstra NA, Grijpma DW, Feijen J, de Groot K, Bezemer JM. Control of vitamin B12 release from poly(ethylene glycol)/poly(butylene terephthalate) multiblock copolymers. Biomaterials 2002;23(6):1527–36.
[29] Deschamps AA, Claase MB, Sleijster WJ, de Bruijn JD, Grijpma DW, Feijen J. Design of segmented poly(ether ester) materials and structures for the tissue engineering of bone. J Control Release 2002;78(1–3):175–86.
[30] Mahmood TA, de Jong R, Riesle J, Langer R, van Blitterswijk CA. Adhesion-mediated signal transduction in human articular chondrocytes: the influence of biomaterial chemistry and tenascin-C. Exp Cell Res 2004;301(2):179–88.
[31] van Blitterswijk CA, van de Brink J, Leenders H, Bakker D. The effect of PEO ratio on degradation, calcification and bone bonding of PEO/PBT copolymer (PolyActive). Cell Mater 1993; 3:23–36.
[32] Beumer GJ, van Blitterswijk CA, Ponec M. Degradation behavior of polymeric matrices in (sub)dermal and muscle tissue of the rat: a quantitative study. Biomaterials 1994;15:551–9.
[33] Beumer GJ, van Blitterswijk CA, Ponec M. Biocompatibility of degradable matrix induced as a skin substitute: an in vivo evaluation. J Biomed Mater Res 1994;28:545–52.
[34] Bakker D, van Blitterswijk CA, Hesseling SC, Grote JJ, Deams WT. Effect of implantation site on phagocyte/polymer interaction and fibrous capsule formation. Biomaterials 1988; 9:14–21.
[35] Mensik I, Lamme EN, Riesle J, Brychta P. Effectiveness and safety of the PEGT/PBT copolymer scaffold as dermal substitute in scar reconstruction wounds (feasibility trial). Cell Tissue Bank 2002;3(4):245–53.

[36] Bulstra SK, Geesink RG, Bakker D, Bulstra TH, Bouwmeester SJ, van der Linden AJ. Femoral canal occlusion in total hip replacement using a resorbable and flexible cement restrictor. J Bone Joint Surg Br 1996;78(6):892–8.
[37] Jones DS. Dynamical mechanical analysis of polymeric systems of pharmaceutical and biomedical significance. Int J Pharm 1999; 179:167–78.
[38] Lewis G. Key issues involved with the use of miniature specimens in the characterization of the mechanical behaviour of polymeric biomaterials —a review. J Biomed Mater Res (Appl Biomater) 2002;63:455–66.
[39] Meyvis TKL, Stubbe BG, van Steenbergen MJ, Hennink WE, De Smedt SC, Demeester J. A comparison between the use of dynamic mechanical analysis and oscillatory shear rheometry for the characterisation of hydrogels. Int J Pharm 2002;244:163–8.
[40] Nazhat SN, Kellomäki M, Törmälä P, Tanner KE, Bonfield W. Dynamic mechanical characterization of biodegradable composites of hydroxyapatite and polylactides. J Biomed Mater Res (Appl Biomater) 2001;58:335–43.
[41] Menard KP. Dynamic mechanical analysis. A practical introduction. Boca Raton: CRC Press LLC; 1999.
[42] Malda J, Woodfield TBF, van der Vloodt F, Wilson C, Martens DE, Tramper J, van Blitterswijk CA, Riesle J. The effect of PEGT/PBT scaffold architecture on the composition of tissue engineered cartilage. Biomaterials 2004;26(1):63–72.
[43] Du C, Klasens P, Haan RE, Bezemer J, Cui FZ, de Groot K, Layrolle P. Biomimetic calcium phosphate coatings on polyactive 1000/70/30. J Biomed Mater Res 2002;59(3):535–46.
[44] Mazzucco D, McKinley G, Scott RD, Spector M. Rheology of joint fluid in total knee arthroplasty patients. J Orthop Res 2002;20:1157–63.
[45] Jurvelin JS, Buschmann MD, Hunziker EB. Optical and mechanical determination of Poisson's ratio of adult bovine humeral articular cartilage. J Biomech 1997;30(3):235–41.